THE JOURNAL OF PHYSICAL CHEMISTRY A
A JOURNAL OF THE AMERICAN CHEMICAL SOCIETY

pubs.acs.org/JPCA

Article

Cutting through the Noise: Extracting Dynamics from Ultrafast Spectra Using Dynamic Mode Decomposition

Published as part of The Journal of Physical Chemistry A virtual special issue "Machine Learning in Physical Chemistry Volume 2".

Cong Xu and Carlos R. Baiz*

Cite This: *J. Phys. Chem. A* 2023, 127, 9853−9862

Read Online

ACCESS | Metrics & More | Article Recommendations | Supporting Information

ABSTRACT: Coherent multidimensional spectroscopy provides experimental access to molecular structure and subpicosecond dynamics in solution. Dynamics are typically inferred from the evolution of lineshapes over a function of waiting time. Numerous spectral analysis methods, such as center/nodal line slope, have been developed to extract these dynamics. However, the extracted dynamics can depend heavily on subjective choices, such as the region selected for CLS analysis or the chosen models. In this study, we introduce a novel approach to extracting dynamics from ultrafast two-dimensional infrared (2D IR) spectra by using dynamic mode decomposition (DMD). As a data-driven method, DMD directly extracts spatiotemporal structures from the complex 2D IR spectra. We evaluated the performance of DMD in simulated and experimental spectra containing overlapped peaks. We show that DMD can retrieve the dynamics of overlapped transitions and cross peaks that are typically challenging to extract with traditional methods. In addition, we demonstrate that combining conditional generative adversarial neural networks with DMD can recover dynamics even at low signal-to-noise ratios. DMD methods do not require preliminary assumptions and can be readily extended to other multidimensional spectroscopies.

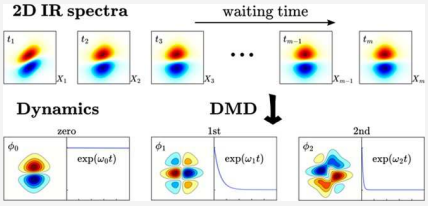

INTRODUCTION

Coherent multidimensional spectroscopy can access the molecular structure and dynamics with femtosecond time resolution. Generally, experimental observables are comprised of lineshapes, amplitudes, polarizations, and time scales.[1−3] Extracting relevant temporal evolution and linking experimental measurements to the underlying dynamics of molecular systems remain key challenges for several reasons: (1) data sets are often highly dimensional containing multiple frequency/time axes, as well as other experimental variables such polarization geometries, or sample conditions such as temperature, (2) complex lineshapes or overlapping bands complicate feature extraction, and (3) experimental noise or artifacts such as scatter are particularly difficult to avoid in certain challenging samples, namely, dilute or highly scattering samples.

Over the past two decades, numerous metrics have been developed to analyze the relationship between time series spectra and molecular dynamics. For example, in two-dimensional infrared (2D IR) spectroscopy,[4,5] proposed methods include the short-time slope of the echo intensity or amplitude,[6] peak shifts,[7,8] dynamic line width,[9] ellipticity,[10] Inhomogeneity Index (II),[11] covariance and skewness,[12] nodal line slope (NLS),[13,14] center line slope (CLS),[15] global fitting to the entire set of time-ordered spectra,[16] pseudo-Zernike Polynomials decomposition[17] and machine learning (ML) iterative reconstruction.[18] Each of these techniques aims to extract the underlying molecular frequency−frequency correlation functions (FFCF).

Among these methods, CLS is the most widely adopted due to its ease of implementation.[19] However, CLS analysis has two important limitations: (1) unreliability in characterizing overlapping peaks and (2) the requirement of relatively high signal-to-noise ratios (SNRs) in the 2D IR spectra, which can translate to long data acquisition times.[20] Recently, the Kubo model-based global fitting has garnered interest for its robustness in noisy systems and its ability to disentangle partially overlapping peaks.[21−24] Despite its high performance in certain experimental systems, Kubo fittings with numerous parameters are subject to standard multivariate fitting issues, such as overfitting or increased risk of multicollinearity. In contrast to many metrics used to extract FFCF, which primarily rely on geometric peak shapes, the Inhomogeneity Index (II) utilizes the amplitudes of both rephasing and nonrephasing signals. Recent studies have indicated that II offers superior performance with systems characterized by narrower line widths or unconventional line

Received: August 25, 2023
Revised: October 20, 2023
Accepted: October 23, 2023
Published: November 9, 2023

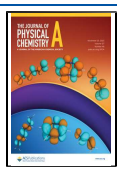

shapes.[25] As a promising tool for evaluating spectral diffusion in complex or noisy systems, II necessitates employing noncollinear geometry or implementing phase cycling within a pump−probe setup.

In this study, we present a novel spectral analysis based on dynamic mode decomposition (DMD), which combines two key advantages: (1) dimensionality reduction of large data sets to suppress noise and extract underlying correlations within variables and (2) extraction of time scales without a priori knowledge of the system or any predefined models. A schematic representation of the DMD approach is depicted in Scheme 1.

Scheme 1. Representation of the Dynamic Mode Decomposition (DMD) Approach Described Here[a]

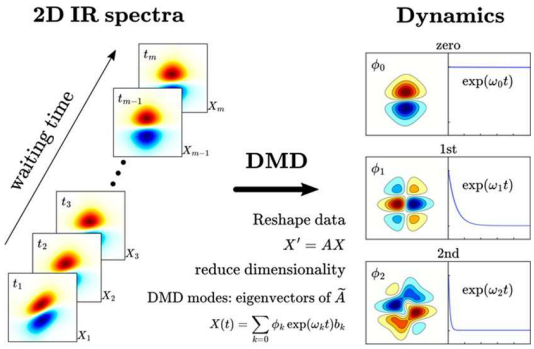

[a]Data set corresponds to a series of simulated 2D IR spectra as a function of waiting time. The output of the method shows the three most important dynamic modes, plotted in the same frequency axes as the input spectra, along with the corresponding exponential time scales associated with each mode.

We begin this paper by introducing the DMD and augmented DMD algorithms. We then test their performance on spectra with varying levels of noise generated using the Kubo line shape model but incorporating experimental laser intensity fluctuations. We apply DMD to simulated spectra with partially overlapped peaks and test the method on experimental temperature-dependent 2D IR spectra of ethyl acetate (EtOAc) in water, demonstrating its ability to discern correlation between individual peaks. This new method demonstrates equivalent performance to established line shape analysis methods when dealing with simple spectra and additionally provides valuable information about overlapped secondary transitions.

METHODS

DMD Applications to 2D IR Spectroscopy. DMD is a dimensionality reduction algorithm designed to decompose time-evolving high-dimensional data into distinct spatiotemporal modes.[26] DMD has found applications across a range of disciplines, including neuroscience,[27] robotics,[28] video compression,[29] and finance.[30] The core concept of DMD is the linear decomposition of discretely sampled time series data into spatially coherent structures whose temporal evolution is described by oscillations or exponential growth/decay.[31] DMD is ideally suited to describe the complex temporal evolution of multidimensional spectra into interpretable components. To demonstrate the use of DMD in the context of 2D IR spectral diffusion, we begin with a series of 2D IR spectra at evenly sampled waiting times, labeled (t_1, t_2,..., t_m). Each spectrum is reshaped to a high-dimensional single-column vector $\mathbf{x}_i$, and all vectors are then assembled into a matrix. This matrix contains the same data as the original spectra. The waiting-time evolution of spectra may follow dynamics described as a nonlinear operator, such that $\frac{d\mathbf{x}}{dt} = \mathbf{f}(\mathbf{x}, t)$, which can be written as $\mathbf{x}_{k+1} = \mathbf{F}(\mathbf{x}_k)$ in discrete-time formalism. DMD approximates solutions to the time-evolution operator by constructing a locally linear dynamical system: $\frac{d\mathbf{x}}{dt} = \mathbf{A}\mathbf{x}$, where $\mathbf{A}$ represents a time-evolution matrix. This linear differential equation has a general solution:

$$\mathbf{x}(t) = \sum_{k=1}^{n} \boldsymbol{\phi}_k \exp(\omega_k t) b_k = \boldsymbol{\Phi} \exp(\boldsymbol{\Omega} t)\mathbf{b} \tag{1}$$

where $\boldsymbol{\phi}_k$ and ω_k are eigenvectors and eigenvalues of $\mathbf{A}$, n is the dimension of the matrix, and the coefficients b_k represent the initial state $\mathbf{x}(0)$. The general solution for a discretely sampled system written as $\mathbf{x}_{k+1}=\mathbf{A}\mathbf{x}_k$ is

$$\mathbf{x}_k = \sum_{j=1}^{r} \boldsymbol{\phi}_j \lambda_j^{\,k} b_j \tag{2}$$

where $\boldsymbol{\phi}_k$ and λ_k are eigenvectors and eigenvalues of discrete-time evolution matrix $\mathbf{A}$, and $\mathbf{b}$ represents the initial state, such that $\mathbf{x}_1=\boldsymbol{\Phi}\mathbf{b}$. This solution is based on locally linear approximation but can approximate nonlinear dynamics if we globally fit the measured data $\mathbf{x}_k$ for $k = 1,2,...,m$ so that the two-norm of the difference between $\mathbf{F}(\mathbf{x}_k)$ and $\mathbf{A}\mathbf{x}_k$ $\|\mathbf{F}(\mathbf{x}_k) - \mathbf{A}\mathbf{x}_k\|_2$ is minimized. One approach is to assemble columns $\mathbf{x}_1$ to $\mathbf{x}_{m-1}$ in the data matrix $\mathbf{X}$, and data column $\mathbf{x}_2$ to $\mathbf{x}_m$ in the shifted data matrix $\mathbf{X}'$ (see Scheme 1). In DMD, the best-fit linear operator $\mathbf{A}$ that satisfies $\mathbf{X}' \approx \mathbf{A}\mathbf{X}$ is computed by $\mathbf{A} = \mathbf{X}'\mathbf{X}^{\dagger}$, where $\mathbf{X}^{\dagger}$ is the Moore−Penrose pseudo-inverse of data matrix $\mathbf{X}$. This solution minimized the error $\|\mathbf{X}' - \mathbf{A}\mathbf{X}\|_2$, where $\|\cdot\|_2$ is the two-norm given by $\|\mathbf{X}\|_2 = \sqrt{\sum_n \sum_m X_{nm}^{\,2}}$. However, this pseudo-inverse matrix is not always well conditioned, so in practice, a dimensionality reduction approach is necessary to describe the A matrix in a reduced space. Typical algorithms to compute DMD proceed as following:

Algorithm 1 (DMD).

1. Compute the single value decomposition (SVD) of the data matrix $\mathbf{X} \in \mathbb{C}^{n\times m}$

$$\mathbf{X} = \mathbf{U}\boldsymbol{\Sigma}\mathbf{V}^{*} \tag{3}$$

2. Perform a low-rank truncation of the data. Obtain $\mathbf{U}_r$, $\boldsymbol{\Sigma}_r$, $\mathbf{V}_r$ by only considering the first r columns of $\mathbf{U}$ and $\mathbf{V}$, and the first r rows and columns of $\boldsymbol{\Sigma}$ where $\mathbf{U}_r \in \mathbb{C}^{n\times r}$, $\boldsymbol{\Sigma}_r \in \mathbb{C}^{r\times r}$, $\mathbf{V}_r \in \mathbb{C}^{m\times r}$.
3. Compute $\tilde{\mathbf{A}}$, the $r \times r$ projection of the full data operator $\mathbf{A}$ into a reduced dimensionality space:

$$\tilde{\mathbf{A}} = \mathbf{U}_r^{*}\mathbf{A}\mathbf{U}_r = \mathbf{U}_r^{*}\mathbf{X}'\mathbf{V}_r\boldsymbol{\Sigma}_r^{-1} \tag{4}$$

4. Compute eigenvalues μ_i and eigenvectors w_i of $\tilde{\mathbf{A}}$, where $\tilde{\mathbf{A}}w_i = \lambda_i w_i$.
5. Every DMD mode ϕ_i with a nonzero eigenvalue μ_i can be written as

$$\boldsymbol{\phi}_i = \lambda_i^{-1}\mathbf{X}'\mathbf{V}_r\boldsymbol{\Sigma}_r^{-1}w_i \tag{5}$$

https://doi.org/10.1021/acs.jpca.3c05755
J. Phys. Chem. A 2023, 127, 9853−9862

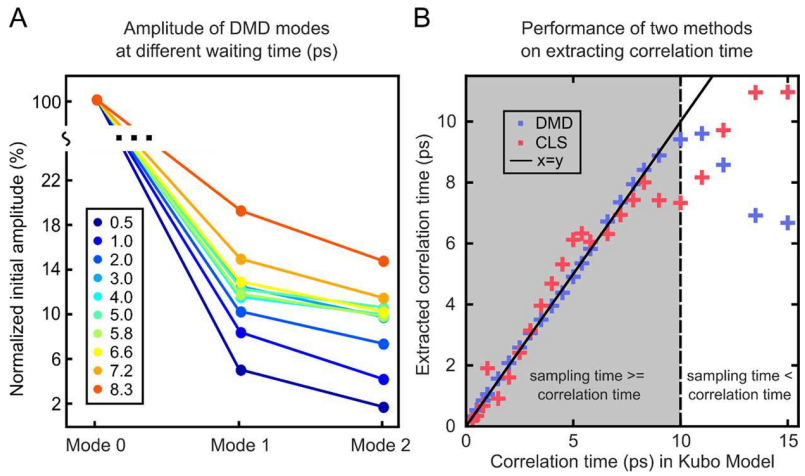

Figure 1. (A) Initial amplitudes (b_i) of the first three DMD modes when extracting different correlation times (picoseconds) in the Kubo model (picoseconds, color code in the inset). Values are normalized by the amplitude of zero mode. (B) Comparison between CLS and DMD retrieval methods for the simulated spectra. The simulated spectra data are generated between 0 and 10 ps, while the correlation time in the Kubo model varies from 0 and 15 ps. Decay times extracted by DMD show better agreement and less variance than CLS if the generated spectra fully capture the entire dynamic process, particularly when the correlation time is longer than the maximum waiting time.

6. To extract the characteristic time constants τ_i describing the evolution of spectra, we need to convert the discrete-time eigenvalues λ_i to continuous eigenvalues ω_i using $\omega_i = \ln(\lambda_i)/\Delta t$, where Δt is the sampling time interval.[32,33] The exponential decay/growth rate τ_i and oscillation frequency ω'_i are given by $\omega_i = \tau_i + i\omega'_i$. The DMD modes associated with each time scale are plotted to visualize the spectral features described by each time scale.
7. Finally, if desired, the reconstruction of 2D spectra at any given time can be written as

$$\mathbf{x}(t) = \sum_{i=1}^{r} \boldsymbol{\phi}_i \exp(\omega_i t)\mathbf{b}_i \tag{6}$$

Algorithm 2 (Augmented DMD). The data matrix can be written as $\mathbf{X} = [\boldsymbol{x}_1 \boldsymbol{x}_2 \cdots \boldsymbol{x}_{m-1}]$, $\mathbf{X}' = [\boldsymbol{x}_2 \ \boldsymbol{x}_3 \ \cdots \ \boldsymbol{x}_m]$. However, we can augment the data matrix by stacking the state $\boldsymbol{x}_i$ with copies of future measurements $x_{i+1}, x_{i+2}, \ldots, x_{i+s}$. Then, we can implement the above DMD method to include the s time-shifted state data matrix:

$$\mathbf{X}_{\text{aug}} = \begin{bmatrix} \boldsymbol{x}_1 & \boldsymbol{x}_2 & \cdots & \boldsymbol{x}_{m-s} \\ \boldsymbol{x}_2 & \boldsymbol{x}_3 & \cdots & \boldsymbol{x}_{m-s+1} \\ \vdots & \vdots & \ddots & \vdots \\ \boldsymbol{x}_s & \boldsymbol{x}_{s+1} & \cdots & \boldsymbol{x}_{m-1} \end{bmatrix} \tag{7}$$

$$\mathbf{X}'_{\text{aug}} = \begin{bmatrix} \boldsymbol{x}_2 & \boldsymbol{x}_3 & \cdots & \boldsymbol{x}_{m-s+1} \\ \boldsymbol{x}_3 & \boldsymbol{x}_4 & \cdots & \boldsymbol{x}_{m-s+2} \\ \vdots & \vdots & \ddots & \vdots \\ \boldsymbol{x}_{s+1} & \boldsymbol{x}_{s+2} & \cdots & \boldsymbol{x}_m \end{bmatrix} \tag{8}$$

A set of modes $\boldsymbol{\phi}_{\text{aug}}$ and corresponding exponential decay rates τ_{aug} can be extracted by performing DMD on the augmented matrix $\mathbf{X}_{\text{aug}}$ and $\mathbf{X}'_{\text{aug}}$. The remainder of the analysis follows the same steps as conventional DMD described above.

Kubo Model Spectra. Simulated 2D IR spectra are generated to test the DMD model. The advantage of using simulated spectra is that the correlation time is an input parameter that can be used to test the performance of DMD in extracting this parameter. Within this study, spectra are generated using the Kubo line shape response function approach. The use of the Kubo model within our study was based on two reasons: (1) Kubo model is a well-established method for generating simulated 2D IR spectra.[18,21] (2) The FFCF in Kubo line shape functions is built on multiple exponential functions. This aligns well with DMD, which is optimized for analyzing such an exponential behavior. However, for complex systems exhibiting nonexponential dynamics,[34] DMD modes may not align with actual physical processes.

In brief, we use six independent parameters to describe 2D IR spectra for a single anharmonic oscillator: anharmonicity (Δ), amplitude (χ), center frequency (ω), frequency fluctuation amplitude ($\Delta\omega$), excited state lifetime (T_1), and correlation time (τ_c). The parameters used here to generate spectra are representative of measured spectra for carbonyl vibrational modes in a molecule experiencing an environment representative of a polar solvent; however, the approach is completely general, and the performance should be comparable for other vibrational modes. In addition, experimental noise was introduced into the simulated spectra by recording blank probe shots from the experimental 2D IR spectrometer.[35] Experimental noise spectra are generated and then added to varying levels, as described previously. The code can be found on GitHub.[36] The parameters used for the Kubo model 2D IR spectra are listed in Table S1.

RESULTS AND DISCUSSION

Case 1: Single Oscillator Model. We first examine the performance of DMD for extracting the correlation time from 2D IR spectral evolution using simulated spectra for a single anharmonic oscillator. Spectral samples were generated at different waiting times, ranging from 100 fs to 10 ps with an interval of 100 fs. Keeping all other parameters constant (Table S1), we vary the correlation time (τ_c) from 0.1 to 15 ps to generate 25 sets of sample spectra (Figure S1). We tested the performance of DMD in comparison to the well-established CLS analysis method. Both retrieval methods were applied to these 25 data sets to extract the correlation time. An example of

https://doi.org/10.1021/acs.jpca.3c05755
J. Phys. Chem. A 2023, 127, 9853−9862

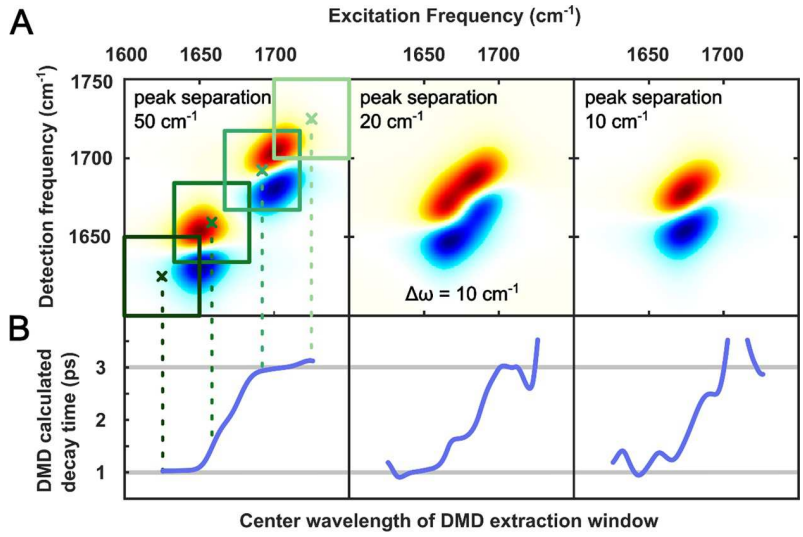

Figure 2. (A) Simulated spectra with different peak separations (50, 20, and 10 cm^{-1}). Two peaks are generated within a 150-wavenumber-wide region. The diagonal width ($\Delta\omega$) of both peaks is 10 cm^{-1} for all spectra. The extraction window used in the DMD algorithm is 50 cm^{-1} in width scanned along the diagonal with an interval of 1 cm^{-1}. Four representative windows (colored green) are shown in the first spectrum. (B) Correlation time (τ_c) for low-frequency peak and high-frequency peak are set to 1 and 3 ps (gray horizontal line) in the Kubo model. The decay times extracted by the different diagonal windows are shown in blue lines. Moving the window along the diagonal shows a transition between the fast and slow correlation times.

extracted DMD mode amplitudes is shown in Scheme 1, and the performance comparison is depicted in Figure 1.

Similar to SVD, the zero (static) mode of DMD has the largest initial amplitude (b_i), normalized to 1 in Figure 1A for all of the data sets. The initial amplitude of Mode 1 varies from 5 to 18% of the zero mode. The higher initial amplitude in samples with longer correlation time suggests that Modes 1 and 2 are more pronounced when the correlation time is within the sampling time range. The DMD decay rate (τ_i) of Mode 1 accurately captures the frequency−frequency correlation time (τ_c) in the Kubo line shape model (Figure 1B). Mode 0 captures the "static" feature that represents the average spectrum, while the decay rate of Mode 2 is approximately an order of magnitude faster than Mode 1. Thus, it is easy to assign the correlation time to mode 1, $\boldsymbol{\phi}_1$ in this scheme. Interestingly, in the simulated single peak spectra, all of the discrete-time eigenvalues λ_i are real and negative, indicating that only exponentially decaying modes exist in this scenario, as expected in the Kubo model where no oscillations are present along the waiting time. In spectra containing multiple peaks and noisy peak spectra, the eigenvalues λ_i may be complex numbers. In complex systems with multiple decay time scales or various pathways, each decay typically appears as a separate DMD mode. However, if a decay rate is very similar to the rate of an FFCF mode, these modes might merge into a single decay. While this could skew the interpretation of individual DMD modes, the overall FFCF decay rate remains relatively stable because the two rates are so alike. It is also important to note that traditional methods are also unable to distinguish between relaxation pathways with similar time constants.

The correlation time extracted by CLS can be influenced by the selected region. In this study, we present CLS results by considering only the maximum intensity in the range of 1660−1690 cm^{-1} in excitation frequency (see sample CLS analysis in Figure S2). The CLS-extracted correlation time is also in good agreement with the input time in the simulated spectra. Interestingly, some small deviations occur possibly as a result of numerical noise or fitting with discretely sampled frequencies. When the correlation time is shorter than the maximum waiting time (0−10 ps), DMD performs significantly better than CLS, as the average variance of the extracted decay time relative to the actual correlation time is less than 0.5% in DMD, compared to 3−5% in CLS. This could be attributed to DMD using all the points in the spectra, whereas CLS only uses a few spectral points. This difference is more pronounced when the correlation time is longer than half of the sampling time (5−10 ps). However, if the correlation time extends beyond the sampling time, then DMD performance deteriorates and fails to capture the dynamics (10−15 ps) due to insufficient waiting time sampling.

Case 2: Overlapping Transitions. The complexity of 2D IR spectra increases significantly when overlapping bands are present. Overlapping transitions with different correlation times, widths, and anharmonicities complicate the CLS analysis and require some additional knowledge of the system.[37] In this study, we demonstrate the applicability of the DMD method for extracting the correlation time of two partially overlapping peaks by analyzing subregions along the diagonal. Spectra are generated with different levels of overlap to assess the performance of DMD and to be able to extract the correlation times of the individual peaks.

Two vibrational bands are generated within the 1600−1750 cm^{-1} range without cross peaks. Both peaks share the same Kubo line shape parameters except for the correlation time: the lower frequency peak has a correlation time of 1 ps, while the higher frequency peak has a correlation time of 3 ps. Among these parameters, the diagonal width ($\Delta\omega$) is set to 10 cm^{-1}. Representative spectra are shown in Figure A; these spectra correspond to relatively separated, partially overlapped, and highly overlapped diagonal peaks.

A 50 cm^{-1} wide window is used to extract the correlation time via DMD. This window is scanned along the diagonal as shown in Figure 2B. In the case of separated peaks, subsection DMD captures two distinct decay times at 1 and 3 ps. This

https://doi.org/10.1021/acs.jpca.3c05755
J. Phys. Chem. A 2023, 127, 9853−9862

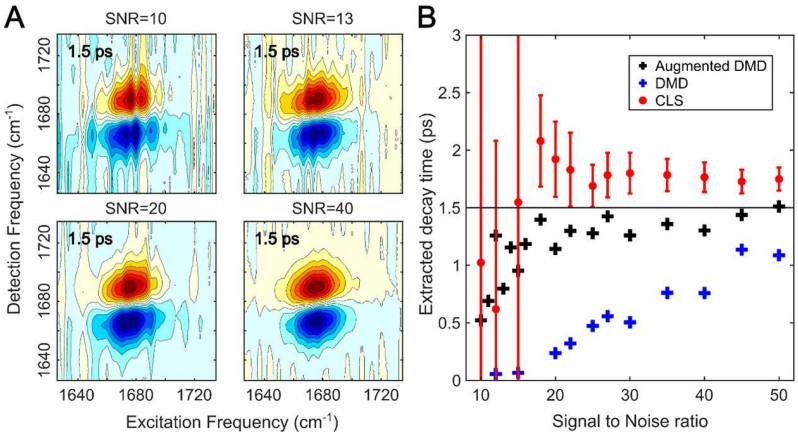

Figure 3. (A) Example simulated spectra generated by the Kubo model at different signal-to-noise ratios (SNRs). The noisy spectra are generated using experimental shot-to-shot fluctuations as described previously.[18] (B) Time constant extracted by CLS/DMD/augmented DMD. The correlation time of 1.5 ps used in the Kubo model shown as a solid line. CLS results are shown with red dots, and their error bars originate from the 95% confidence interval of the exponential fits. The exponential decay rates of Mode 1 for standard DMD and augmented DMD are indicated by blue and black cross marks, respectively.

demonstrates that if peaks are well-separated, then DMD can extract dynamics precisely as long as part of the peak falls within the range of the extraction window. DMD analysis applied to partially overlapped peaks reflects the correct correlation near the edges of both peaks (1660 and 1700 cm^{-1}). However, in the overlapped area (1665−1675 cm^{-1}), an intermediate decay time of 1.5 ps emerges, possibly resulting from the mixed dynamics of both peaks. In highly overlapped peaks, where peak separation equals the diagonal width (10 cm^{-1}), the extracted decay time at the edges of the peaks (1665 and 1695 cm^{-1}) is no longer accurate (1.3 and 2.5 ps). The intensity change at the edge of the second peak is not negligible, even at the center of the first peak. Nevertheless, subsection DMD qualitatively captures the fast and slow correlation times despite the high overlap between the two peaks such that they appear as a single feature in the 2D spectra.

It is important to note that the window width should be carefully selected depending on the system as it has some influence on the DMD-extracted decay time. If the window is smaller than the full width at half-maximum (fwhm) of the individual peak, the extracted decay time will fluctuate around the correlation time when the window is scanned along the diagonal axis. In contrast, an appropriately sized window of approximately the fwhm of the peak yields a stable result close to the correlation time. Additionally, a window only captures the tail of the peak can sometimes result in divergent correlation times due to numerical noise as illustrated in the rightmost example in Figure 2B.

Case 3: Simulated Spectra with Noise. One potential shortcoming of the DMD algorithm is its susceptibility to noise, which systematically biases the eigenvalues.[38] A variety DMD extensions have been explored to address this issue, including the total least-squares DMD (TLS-DMD)[39] and forward−backward DMD (fb-DMD).[40] In this study, we apply the DMD algorithm to augmented data sets and achieve satisfactory performance on the simulated spectra with relatively high levels of noise.

Given that 2D IR spectra are collected by recording differences between individual laser shots, the main source of noise arises from shot-to-shot fluctuations of the probe.[41,42] These fluctuations are attributed to fluctuations in the laser output intensity as well as the 2D IR optical setup, such as air currents and optomechanical drift. Within each SNR, 200 simulated spectra are generated with uniformly distributed waiting times ranging from 150 to 3000 fs. The noisy spectra are generated by combing the Kubo line shape generated spectra with the experimental collected shot-to-shot noise.[18] Here, the SNR is defined as the ratio of the maximum amplitude of the Kubo line shape generated spectra (across all time delays) to the root-mean-square amplitude of the noise floor.

The CLS analysis demonstrates resilience to systematic noise: the deviation in the extracted dynamics is less than 15% when the SNR exceeds 20 (Figure 3). CLS methods appear to be reliable when the SNR is greater than ∼15. Intriguingly, the decay time extracted by CLS is about 20% longer than the actual value (1.5 ps). On the contrary, the standard DMD method exhibits considerable sensitivity to noise. DMD modes capture the fluctuation of shot-to-shot noise patterns, which results in a 50% lower time constant even at a high SNR of 50. Within a low SNR of 10−20, the DMD's fundamental mode is likely to be completely dominated by shot-to-shot noise variations, leading to an unreliable extracted decay time.

In our implementation of Augmented DMD, the data matrix is constructed by stacking adjacent spectra together into the matrix, following eqs 7 and 8:

$$\mathrm{X}_{\mathrm{aug}} = \begin{bmatrix} x_1 & x_2 & & x_{m-5} \\ x_2 & x_3 & & x_{m-4} \\ x_3 & x_4 & \cdots & x_{m-3} \\ x_4 & x_5 & & x_{m-2} \\ x_5 & x_6 & & x_{m-1} \end{bmatrix}, \mathrm{X'}_{\mathrm{aug}} = \begin{bmatrix} x_2 & x_3 & & x_{m-4} \\ x_3 & x_4 & & x_{m-3} \\ x_4 & x_5 & \cdots & x_{m-2} \\ x_5 & x_6 & & x_{m-1} \\ x_6 & x_7 & & x_m \end{bmatrix} \tag{9}$$

where $\boldsymbol{x}_i$ represents the reshaped spectrum taken at ith time delay. Since the propagation operator $\mathbf{A}$ of the augmented data matrix transits ith state to $(i + 1)$th state, i.e.,

https://doi.org/10.1021/acs.jpca.3c05755
J. Phys. Chem. A 2023, 127, 9853−9862

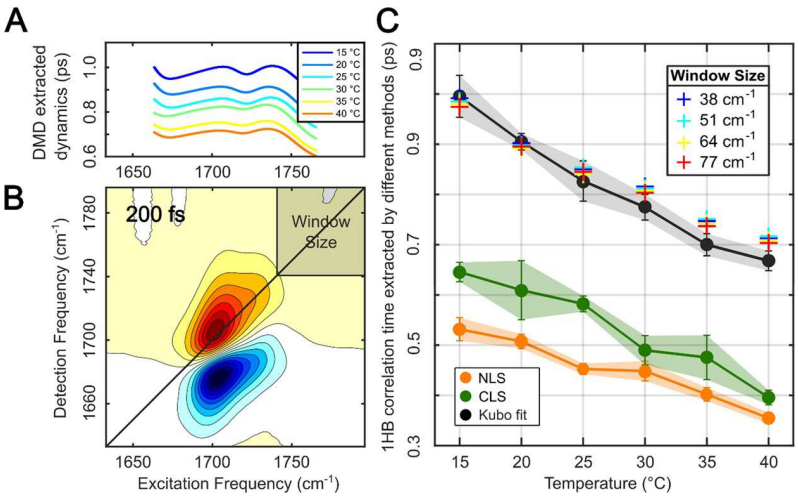

Figure 4. (A) Frequency-dependent time constant of augmented DMD Mode 1 for each of the temperature-dependent waiting-time 2D IR spectra. (B) Example 2D IR spectrum of 10 mg/mL EtOAc D_2O solution measured at 25 °C and 200 fs waiting time. The DMD extraction window is colored gray. (C) Round dot stands for the correlation time extracted by traditional methods, such as CLS, NLS, and fitting the spectra line shape to the Kubo model. The crosshairs show the averaged DMD correlation time using different extraction window sizes varying from 38 to 77 cm^{-1} as indicated in the figure. The plot shows that the size of the window has essentially no impact on the extracted DMD time constant.

$$\mathrm{X}_i = \begin{bmatrix} x_i \\ x_{i+1} \\ x_{i+2} \\ x_{i+3} \\ x_{i+4} \end{bmatrix} \rightarrow \mathrm{X}_{i+1} = \begin{bmatrix} x_{i+1} \\ x_{i+2} \\ x_{i+3} \\ x_{i+4} \\ x_{i+5} \end{bmatrix} \tag{10}$$

simultaneously, it considerably reduces the noise fluctuations captured. As shown in Figure 3B, the exponential decay constants of augmented DMD Mode 1 are within 10% of 1.5 ps for SNR >20, demonstrating much greater stability against shot-to-shot noise than the standard DMD. When SNR falls below 15, augmented DMD modes become noisy. In conclusion, the performance of the augmented DMD against noisy spectra is on par with the CLS methods.

Case 4: Experimental Spectra of a Carbonyl. In this section, we assess the performance of DMD using experimental data with two partially overlapped peaks. The data set consists of temperature-dependent 2D IR spectra of the ethyl acetate (EtOAc) ester carbonyl mode. The samples consist of 10 mg/mL EtOAc in D_2O at 15, 20, 25, 30, 35, and 40 °C. The waiting times are uniformly distributed from 100 to 2000 fs with an interval of 100 fs. Uniform sampling is required for standard DMD, though new approaches are able to estimate DMD modes from nonuniformly sampled data.[43,44] The carbonyl stretch region of EtOAc shows two peaks attributed to the one H-bond and two H-bond configurations.[45] The peaks are separated by 15 cm^{-1}, and the diagonal widths are 15−20 cm^{-1}. H-bond exchange can also result in the presence of cross peaks.[46] The DMD-extracted time constants are compared to CLS, NLS, and numerical fitting to a two-oscillator Kubo line shape model as previously described.[21]

The low-frequency 2 H-bond peak (~1695−1710 cm^{-1}) is the strongest feature observed in the 2D IR spectrum (Figure 4B). Similarly, this peak has the highest intensity in the FTIR spectrum (Figure S5). Thus, this frequency region is used for the CLS and NLS analysis of the data shown in Figure 4. The NLS-extracted dynamics display a consistent trend, ranging from 0.5 to 0.3 ps with increasing temperature from 15 to 40 °C. The CLS results are similar but exhibit 20% slower, from 0.6 to 0.4 ps. The error bars in CLS and NLS fits show a 95% confidence interval from the single-exponential fits (Figures S12 and S13). In the Kubo model fits, the parameters are optimized to minimize the sum of the mean square errors of the spectra across all time delays. The temperature-dependent correlation extracted from the Kubo model fits are shown in Figure 4D. The dynamics derived from the Kubo fits follow the same trend as CLS or NLS, but the decay times are approximately twice as slow as those extracted in NLS, ranging from 1.0 to 0.7 ps.

The augmented DMD algorithm is applied by using a variable-size window scanned along the diagonal (see Figure 4B,C). The time constants of Mode 1, relative to the center of the window, are shown in Figure 4A. The dynamics of the low-frequency peak are ascertained by averaging the exponential constants of Mode 1 while scanning the center of the window from 1695 to 1710 cm^{-1}, corresponding to the same region analyzed using the CLS and NLS methods above. We tested various subsection window sizes ranging from 38 to 77 cm^{-1}. The DMD time constants within the center region of the spectrum (1680−1750 cm^{-1}) display remarkable consistency with respect to the window size (see Figure 4C and S14). The performance of DMD remains notably stable, provided that the chosen analysis window can distinguish different transitions and avoid low-amplitude regions of the spectrum.

Interestingly, the temperature-dependent 1 H-bond dynamics extracted DMD and Kubo model fits are very consistent (1.0 to 0.7 ps) but are both slower than those obtained through CLS and NLS methods (0.7 to 0.4 ps). The partial overlap between the 1 and 2 H-bond peaks is likely to be an important factor in this discrepancy as both CLS and NLS only apply to single peaks, but the two-oscillator Kubo model and DMD are able to extract dynamics when peaks are partially overlapped. Furthermore, the correlation time of the high-frequency (1 H-bond peak) is slower than the low-frequency (2 H-bond) peak, as expected. The DMD and Kubo fitting methods, which take into account the two peaks separately, are more likely to produce results that accurately reflect the dynamics of the peak of interest.

https://doi.org/10.1021/acs.jpca.3c05755
J. Phys. Chem. A 2023, 127, 9853−9862

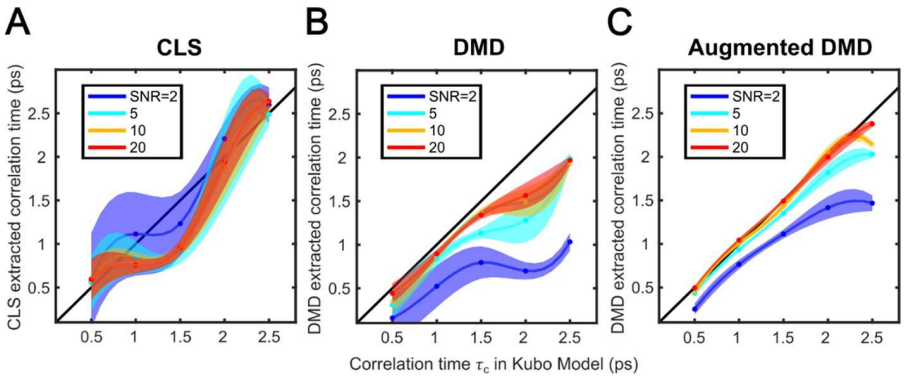

Figure 5. (A) CLS correlation time extracted from cGANNs recovered spectra whose SNR equals 2, 5, 10, and 20. The horizontal axis represents the correlation lifetime used in the Kubo generating model, and the vertical axis represents the extracted correlation lifetime. The error bars represent a 95% confidence level monoexponential fit. The CLS-extracted correlation time is within the 30% range of the actual parameters used in the Kubo model. (B) Correlation time was extracted using DMD. In general, DMD produces ∼50% faster correlation times compared to the input parameters. The error bars are calculated based on the standard deviation of three independent sets of simulated spectra denoised independently using the cGANN method. (C) Correlation times extracted by augmented DMD align very well with the actual correlation time when SNR = 5, 10, and 20.

Case 5: Denoised Spectra Using Machine Learning. The low SNRs inherent to 2D IR spectroscopy present significant challenges and can make certain measurements unfeasible.[47−49] Numerous numerical postprocessing methods have been employed for noise suppression.[50−52] Recently, a ML denoising technique has been introduced using conditional generative adversarial neural networks (cGANNs) to suppress noise in 2D IR spectra by reconstructing the features of the spectra based on a training set.[18] Once trained on simulated spectra, the neural network can retrieve the line shapes from experimental spectra with a SNR of as low as 2:1. In this case study, both CLS and DMD methods are implemented to extract the FFCF from the spectra recovered by the ML technique as an unsupervised learning method, cGANNs consist of a generator neural network that produces sets of spectra and a discriminator designed to distinguish between spectra derived from the training set and those from the generated image set. The training protocol is described in detail in ref 18, and the training data and scripts are available on GitHub,[53] so here we provide a brief summary. In this demonstration, the training set includes five sets of 200 simulated spectra containing SNR of 2, 5,10, and 20, and one set without noise. The noise is generated by measuring "blank" probe shots (i.e., probe shots without 2D IR signal) using the 2D IR setup described above, and the laser shots are used to generate the spectral noise features, which are added to the generated Kubo model spectra at various amplitudes to simulate data at various SNRs.

Single peak series of 2D IR spectra are generated at 200 equally spaced waiting times ranging from 150 to 3000 fs. Five sets of spectra are produced, having identical Kubo parameters (Figure S15) but varying correlation times (τ_c), which range from 0.5 to 2.5 ps. Subsequently, the experimental shot-to-shot noise spectra are added into the simulated spectra. As depicted in Figure 3B, analyzing spectra with an SNR of below 20 becomes challenging. However, by reconstructing "clean" spectra using the trained cGANN, we can recover the lineshapes as demonstrated in Figures S15 and S16, as well as in our previous study.[18] This denoising capability opens opportunities for more accurate and detailed analysis of spectra.

In Figure 5, we evaluate the performance of cGANNs denoised spectra using CLS/DMD methods by applying them to spectra reconstructed from noisy data with SNR values of 2, 5, 10, and 20. Naturally, the CLS shows a monoexponential relaxation, as displayed in Figure S12. The extracted CLS relaxation time is within 30% of the correlation time used in the generating model even at SNR = 2. The error bars are determined by calculating the 95% confidence intervals of the exponential decay fitting. As shown in Figure 5B, the dynamics extracted by DMD are somewhat faster than the Kubo correlation time. However, there are no shot-to-shot noise contributions in the reconstructed spectra, yet the DMD-extracted time scales are significantly faster. We found that because the neural network is trained with randomized peak positions and widths, the peak's center in the cGANN-reconstructed spectra is influenced by the noise in the input spectra. When the SNR is below 10, the peak's center can vary by as much as 5 wavenumbers from one spectrum to another. These fluctuations in peak position are captured by DMD analysis, leading to an acceleration of the extracted dynamics. The loss of monotonicity in the extracted time versus the actual correlation time is also evident at low SNR.

While conventional DMD does not perform well with reconstructed spectra, the time constant extracted by augmented DMD aligns well with correlation time used in spectra generation. When the SNR is 5, fluctuations in peak position cause a 10% acceleration in the extracted dynamics. Compared with CLS, the stability of augmented DMD is enhanced. However, when the SNR drops to 2, the discrepancy in the extracted dynamics increases to 30%, making augmented DMD methods less appealing compared with the CLS approach. In conclusion, when analyzing noisy spectra, if the SNR is greater than 20, applying augmented DMD directly to the spectra proves slightly superior to CLS methods in terms of validity and robustness. If the SNR falls between 20 and 5, requiring preprocessing steps such as SVD cleanup or cGANN reconstruction, augmented DMD is preferred. However, when the SNR drops below 5, the traditional CLS method applied to reconstructed spectra demonstrates greater robustness.

■ DISCUSSION

The DMD methods mentioned above can be applied to analyze the dynamics of a wide range of multidimensional spectra, not limited to 2D IR spectra but also extendable to 2D visible or mixed vibrational and electronic methods. The method has been demonstrated to be robust and can be applied to entire spectra

https://doi.org/10.1021/acs.jpca.3c05755
J. Phys. Chem. A 2023, 127, 9853−9862

or to specific peaks. Based on the current results, we offer some suggestions for the application of DMD methods:

1. Region selection: As shown in Figures 4C and S14, the extracted dynamics constants and the performance of DMD-reconstructed spectra remain consistent regardless of the window size. However, it is crucial to avoid using excessively small sampling windows, such as 10 cm^{-1} windows, as they may not adequately cover the entire region of interest and could cause numerical issues in DMD. The data matrix may lose its tall, skinny shape, affecting the accuracy and stability of the DMD analysis. On the other hand, selecting large windows that encompass multiple transitions may result in dynamic modes that cover multiple transitions, leading to less reliable results. Hence, it is essential to strike a balance and avoid capturing two overlapping transitions, while providing sufficient data for reliable analysis.
2. Truncation rank (R): Similar to SVD, determining the number of singular values to keep, i.e., the truncation rank (R), is a critical factor influencing the performance of DMD. The choice of R depends on various factors, such as the noise level in the data and the importance of low-energy modes. In general, higher noise levels or more significant contributions from low-energy modes may necessitate a higher R value. Figure S3 illustrates that the extracted DMD modes are influenced by the truncation rank. Mode 0, representing the static basis, and Mode 1, depicting the primary exponential decay, remain consistent regardless of R. Furthermore, the time constants of Mode 1 align well with the standard time constant within the range of $R = 4$ to $R = 30$. However, the time constants of Mode 2 or higher exhibit significant variations (Table S1). This suggests that in our test 2D IR data set modes beyond Mode 2 might lack a direct physical interpretation.

   Using too few ranks, such as $R = 5$ in Figure S4, can lead to distorted shapes in the reconstructed spectra, particularly at earlier waiting times. Generally, a singular value threshold is chosen to retain 99% of the total variance in the data. However, in some cases, due to higher noise levels, this may require a larger number of ranks. Nevertheless, excessively large ranks (e.g., $R = 100$) can lead to issues such as the data matrix approaching singularity or displaying poor scaling, resulting in numerical errors. As a popular choice for complicated systems, soft thresholding, where no hard cutoff is applied but instead the low-rank mode amplitudes are smoothly reduced, helps address some of these challenges in selecting the appropriate truncation rank.[54]

It is crucial to carefully examine the reconstructed DMD spectra to validate the choice of the reconstructed region and truncation ranks. This step ensures that the extracted dynamics accurately represent the underlying physical processes and are not influenced by multiple dynamic processes or system noise.

CONCLUSIONS

We demonstrated a new method based on DMD to extract time scales from ultrafast 2D IR spectra. Our results demonstrate that DMD is an effective and robust method to extract dynamics from simulated spectra, experimental spectra with overlapping peaks and cross peaks, and noisy spectra. Comparing to traditional methods, DMD does not rely on prior knowledge or assumptions, and it offers a global consideration of spectra across all time delays, making it suitable to be extended to multidimensional spectroscopy. Moreover, DMD continues to be developed since its original introduction in 2009, with the addition of backward-forward noise canceling DMD in 2015 to eliminate bias from sensor noise[40] and nonuniform sampling DMD in 2016, which allows for analysis of experimental data measured at nonuniform waiting times.[44] Furthermore, the combination of DMD with other data-driven denoising techniques, such as ML algorithms, offers enhanced denoising capabilities. Overall, this work highlights the potential of DMD as a useful tool for the analysis of multidimensional spectra.

ASSOCIATED CONTENT

Supporting Information

The Supporting Information is available free of charge at https://pubs.acs.org/doi/10.1021/acs.jpca.3c05755.

2D IR lineshape model used in simulated spectra generation; CLS analysis applied to simulated spectra; extracted modes, decay rates, and initial amplitudes across various truncation ranks; spectra reconstructed using truncation ranks of 5 and 10; experimental FTIR and 2D IR data of EtOAc in D2O at assorted temperatures; CLS, NLS, and 2D fitting data sets; DMD-reconstructed lineshapes with various subsection window sizes; and simulated noisy spectra and cGANN-reconstructed spectra (SNR = 5) (PDF)

AUTHOR INFORMATION

Corresponding Author

Carlos R. Baiz − *Department of Chemistry, University of Texas at Austin, Austin, Texas 78712, United States;* orcid.org/0000-0003-0699-8468; Email: cbaiz@cm.utexas.edu

Author

Cong Xu − *Department of Chemistry, University of Texas at Austin, Austin, Texas 78712, United States;* orcid.org/0000-0002-7102-2851

Complete contact information is available at: https://pubs.acs.org/10.1021/acs.jpca.3c05755

Notes

The authors declare no competing financial interest.

ACKNOWLEDGMENTS

We gratefully acknowledge financial support from the Welch Foundation (F-1891), NSF-CAREER (CHE-1847199), and the Department of Defense (Army Research Office) through the Multidisciplinary University Research Initiative (Award W911-NF-13-1-0383). C.X. was supported by the James Thompson Graduate Fellowship.

REFERENCES

(1) Hamm, P.; Zanni, M. Concepts and Methods of 2D Infrared Spectroscopy 2011, P23−P25.

(2) Fayer, M. D. Dynamics of Liquids, Molecules, and Proteins Measured with Ultrafast 2D IR Vibrational Echo Chemical Exchange. *Spectroscopy* **2009**, *60*, 21−38.

(3) Xiong, W. Ultrafast Multidimensional Spectroscopy to Probe Molecular Vibrational Polariton Dynamics. *ACS Symp. Ser.* **2021**, *1398*, 89−107.

(4) Baiz, C. R.; Błasiak, B.; Bredenbeck, J.; Cho, M.; Choi, J. H.; Corcelli, S. A.; Dijkstra, A. G.; Feng, C. J.; Garrett-Roe, S.; Ge, N. H.;

et al. Vibrational Spectroscopic Map, Vibrational Spectroscopy, and Intermolecular Interaction. *Chem. Rev.* **2020**, *120* (15), 7152−7218.
(5) Mukamel, S. MULTIDIMENSIONAL FEMTOSECOND CORRELATION SPECTROSCOPIES OF ELECTRONIC AND VIBRATIONAL EXCITATIONS. *Annu. Rev. Phys. Chem.* **2000**, *51*, 691−729.
(6) Piryatinski, A.; Skinner, J. L. Determining Vibrational Solvation-Correlation Functions from Three-Pulse Infrared Photon Echoes. *J. Phys. Chem. B* **2002**, *106* (33), 8055−8063.
(7) De Boeij, W. P.; Pshenichnikov, M. S.; Wiersma, D. A. On the Relation between the Echo-Peak Shift and Brownian-Oscillator Correlation Function. *Chem. Phys. Lett.* **1996**, *253* (1−2), 53−60.
(8) Cho, M.; Yu, J.-Y.; Joo, T.; Nagasawa, Y.; Passino, S. A.; Fleming, G. R. The Integrated Photon Echo and Solvation Dynamics. *J. Phys. Chem.* **1996**, *100* (29), 11944−11953.
(9) Asbury, J. B.; Steinel, T.; Stromberg, C.; Corcelli, S. A.; Lawrence, C. P.; Skinner, J. L.; Fayer, M. D. Water Dynamics: Vibrational Echo Correlation Spectroscopy and Comparison to Molecular Dynamics Simulations. *J. Phys. Chem. A* **2004**, *108* (7), 1107−1119.
(10) Lazonder, K.; Pshenichnikov, M. S.; Wiersma, D. A. Easy Interpretation of Optical Two-Dimensional Correlation Spectra. *Opt. Lett.* **2006**, *31* (22), 3354−3356.
(11) Roberts, S. T.; Loparo, J. J.; Tokmakoff, A. Characterization of Spectral Diffusion from Two-Dimensional Line Shapes. *J. Chem. Phys.* **2006**, *125*, 84502.
(12) Hamm, P. Three-Dimensional-IR Spectroscopy: Beyond the Two-Point Frequency Fluctuation Correlation Function. *J. Chem. Phys.* **2006**, *124* (12), 124506.
(13) Kwac, K.; Cho, M. Two-Color Pump-Probe Spectroscopies of Two-and Three-Level Systems: 2-Dimensional Line Shapes and Solvation Dynamics. *J. Phys. Chem. A* **2003**, *107* (31), 5903−5912.
(14) Demirdöven, N.; Khalil, M.; Tokmakoff, A. Correlated Vibrational Dynamics Revealed by Two-Dimensional Infrared Spectroscopy. *Phys. Rev. Lett.* **2002**, *89* (23), No. 237401.
(15) Kwak, K.; Park, S.; Finkelstein, I. J.; Fayer, M. D. Frequency-Frequency Correlation Functions and Apodization in Two-Dimensional Infrared Vibrational Echo Spectroscopy: A New Approach. *J. Chem. Phys.* **2007**, *127* (12), 124503.
(16) Candelaresi, M.; Gumiero, A.; Adamczyk, K.; Robb, K.; Bellota-Antón, C.; Sangal, V.; Munnoch, J.; Greetham, G. M.; Towrie, M.; Hoskisson, P. A.; et al. A Structural and Dynamic Investigation of the Inhibition of Catalase by Nitric Oxide. *Org. Biomol Chem.* **2013**, *11* (44), 7778−7788.
(17) Gurung, A.; Kuroda, D. G. A New Method Based on Pseudo-Zernike Polynomials to Analyze and Extract Dynamical and Spectral Information from the 2DIR Spectra. *J. Chem. Phys.* **2023**, *159* (3), 34201.
(18) Al-Mualem, Z. A.; Baiz, C. R. Generative Adversarial Neural Networks for Denoising Coherent Multidimensional Spectra. *J. Phys. Chem. A* **2022**, *126* (23), 3816−3825.
(19) Guo, Q.; Pagano, P.; Li, Y. L.; Kohen, A.; Cheatum, C. M. Line Shape Analysis of Two-Dimensional Infrared Spectra. *J. Chem. Phys.* **2015**, *142* (21), 212427.
(20) Van Wilderen, L. J. G. W.; Kern-Michler, D.; Müller-Werkmeister, H. M.; Bredenbeck, J. Vibrational Dynamics and Solvatochromism of the Label SCN in Various Solvents and Hemoglobin by Time Dependent IR and 2D-IR Spectroscopy. *Phys. Chem. Chem. Phys.* **2014**, *16* (36), 19643−19653.
(21) Valentine, M. L.; Waterland, M. K.; Fathizadeh, A.; Elber, R.; Baiz, C. R. Interfacial Dynamics in Lipid Membranes: The Effects of Headgroup Structures. *J. Phys. Chem. B* **2021**, *125* (5), 1343−1350.
(22) Robben, K. C.; Cheatum, C. M. Least-Squares Fitting of Multidimensional Spectra to Kubo Line-Shape Models. *J. Phys. Chem. B* **2021**, *125* (46), 12876−12891.
(23) Johnson, C. A.; Parker, A. W.; Donaldson, P. M.; Garrett-Roe, S. An Ultrafast Vibrational Study of Dynamical Heterogeneity in the Protic Ionic Liquid Ethyl-Ammonium Nitrate. I. Room Temperature Dynamics. *J. Chem. Phys.* **2021**, *154* (13), 134502.
(24) Brinzer, T.; Berquist, E. J.; Ren, Z.; Dutta, S.; Johnson, C. A.; Krisher, C. S.; Lambrecht, D. S.; Garrett-Roe, S. Ultrafast Vibrational Spectroscopy (2D-IR) of CO2 in Ionic Liquids: Carbon Capture from Carbon Dioxide's Point of View. *J. Chem. Phys.* **2015**, *142* (21), 212425.
(25) Duan, R.; Mastron, J. N.; Song, Y.; Kubarych, K. J. Direct Comparison of Amplitude and Geometric Measures of Spectral Inhomogeneity Using Phase-Cycled 2D-IR Spectroscopy. *J. Chem. Phys.* **2021**, *154* (17), 174202.
(26) Schmid, P. J. Dynamic Mode Decomposition of Numerical and Experimental Data. *J. Fluid Mech.* **2010**, *656*, 5−28.
(27) Brunton, B. W.; Johnson, L. A.; Ojemann, J. G.; Kutz, J. N. Extracting Spatial−Temporal Coherent Patterns in Large-Scale Neural Recordings Using Dynamic Mode Decomposition. *J. Neurosci. Methods* **2016**, *258*, 1−15.
(28) Berger, E.; Sastuba, M.; Vogt, D.; Jung, B.; Ben Amor, H. Estimation of Perturbations in Robotic Behavior Using Dynamic Mode Decomposition. *Adv. Rob.* **2015**, *29* (5), 331−343.
(29) Grosek, J.; Nathan Kutz, J. *Dynamic Mode Decomposition for Real-Time Background/Foreground Separation in Video*, 2014, arXiv: 1404.7592.
(30) Mann, J.; Kutz, J. N. Dynamic Mode Decomposition for Financial Trading Strategies. *Quant. Finance* **2016**, *16* (11), 1643−1655.
(31) Wu, Z.; Brunton, S. L.; Revzen, S. Challenges in Dynamic Mode Decomposition. *J. R. Soc. Interface* **2021**, *8* (185), 686 DOI: 10.1098/rsif.2021.0686.
(32) Kutz, J. N.; Brunton, S. L.; Brunton, B. W.; Proctor, J. L. Chapter 1: Dynamic Mode Decomposition: An Introduction. *Dyn. Mode Decompos.* **2016**, P1−P24.
(33) Dawson, S. T. M.; Hemati, M. S.; Williams, M. O.; Rowley, C. W. Characterizing and Correcting for the Effect of Sensor Noise in the Dynamic Mode Decomposition. *Exp. Fluids* **2016**, *57* (3), 42.
(34) Garrett-Roe, S.; Perakis, F.; Rao, F.; Hamm, P. Three-Dimensional Infrared Spectroscopy of Isotope-Substituted Liquid Water Reveals Heterogeneous Dynamics. *J. Phys. Chem. B* **2011**, *115* (21), 6976−6984.
(35) Edington, S. C.; Gonzalez, A.; Middendorf, T. R.; Halling, D. B.; Aldrich, R. W.; Baiz, C. R. Coordination to Lanthanide Ions Distorts Binding Site Conformation in Calmodulin. *Proc. Natl. Acad. Sci. U. S. A.* **2018**, *115* (14), E3126−E3134.
(36) *baizgroup/SyntheticSpectra: Synthetic spectra used in cGANNs and the scripts to generate them.* https://github.com/baizgroup/SyntheticSpectra (accessed 2023-08-24).
(37) Fenn, E. E.; Fayer, M. D. Extracting 2D IR Frequency-Frequency Correlation Functions from Two Component Systems. *J. Chem. Phys.* **2011**, *135* (7), 74502.
(38) Hemati, M. S.; Rowley, C. W.; Deem, E. A.; Cattafesta, L. N. De-Biasing the Dynamic Mode Decomposition for Applied Koopman Spectral Analysis of Noisy Datasets. *Theor. Comput. Fluid Dyn.* **2017**, *31* (4), 349−368.
(39) Golub, G. H.; Loan Van, C. F. An Analysis of the Total Least Squares Problem. *SIAM J. Numer. Anal.* **1980**, *17* (6), 883−893.
(40) Dawson, S. T. M.; Hemati, M. S.; Williams, M. O.; Rowley, C. W. Characterizing and Correcting for the Effect of Sensor Noise in the Dynamic Mode Decomposition. *Exp. Fluids* **2016**, *57* (3), 1−19.
(41) Dunbar, J. A.; Osborne, D. G.; Anna, J. M.; Kubarych, K. J. Accelerated 2D-IR Using Compressed Sensing. *J. Phys. Chem. Lett.* **2013**, *4* (15), 2489−2492.
(42) Brazard, J.; Bizimana, L. A.; Turner, D. B. Accurate Convergence of Transient-Absorption Spectra Using Pulsed Lasers. *Rev. Sci. Instrum.* **2015**, *86* (5), No. 053106, DOI: 10.1063/1.4921479.
(43) Leroux, R.; Cordier, Laurent Dynamic Mode Decomposition for Non-Uniformly Sampled Data. *Exp. Fluids* **2016**, *57*, 94.
(44) Guéniat, F.; Mathelin, L.; Pastur, L. R. A Dynamic Mode Decomposition Approach for Large and Arbitrarily Sampled Systems. *Phys. Fluids* **2015**, *27* (2), 25113.
(45) Edington, S. C.; Flanagan, J. C.; Baiz, C. R. An Empirical IR Frequency Map for Ester C = O Stretching Vibrations. *J. Phys. Chem. A* **2016**, *120* (22), 3888−3896.

(46) Kashid, S. M.; Jin, G. Y.; Chakrabarty, S.; Kim, Y. S.; Bagchi, S. Two-Dimensional Infrared Spectroscopy Reveals Cosolvent-Composition-Dependent Crossover in Intermolecular Hydrogen-Bond Dynamics. *J. Phys. Chem. Lett.* **2017**, *8* (7), 1604−1609.
(47) Schmidt-Engler, J. M.; Blankenburg, L.; Zangl, R.; Hoffmann, J.; Morgner, N.; Bredenbeck, J. Local Dynamics of the Photo-Switchable Protein PYP in Ground and Signalling State Probed by 2D-IR Spectroscopy of − SCN Labels. *Phys. Chem. Chem. Phys.* **2020**, *22* (40), 22963−22972.
(48) Flanagan, J. C.; Baiz, C. R. Site-Specific Peptide Probes Detect Buried Water in a Lipid Membrane. *Biophys. J.* **2019**, *116* (9), 1692−1700.
(49) Ciardi, G.; Berger, A.; Hamm, P.; Shalit, A. Signatures of Intra- And Intermolecular Vibrational Coupling in Halogenated Liquids Revealed by Two-Dimensional Raman-Terahertz Spectroscopy. *J. Phys. Chem. Lett.* **2019**, *10* (15), 4463−4468.
(50) Kübel, J.; Westenhoff, S.; Maj, M. Giving Voice to the Weak: Application of Active Noise Reduction in Transient Infrared Spectroscopy. *Chem. Phys. Lett.* **2021**, *783*, No. 139059.
(51) Auböck, G.; Consani, C.; Monni, R.; Cannizzo, A.; Van Mourik, F.; Chergui, M. Femtosecond Pumpsupercontinuum-Probe Setup with 20 kHz Repetition Rate. *Rev. Sci. Instrum.* **2012**, *83* (9), No. 093105, DOI: 10.1063/1.4750978.
(52) Feng, Y.; Vinogradov, I.; Ge, N.-H.; Chan, W. S.; Yee, T. K. General Noise Suppression Scheme with Reference Detection in Heterodyne Nonlinear Spectroscopy. *Opt. Express* **2017**, *25* (21), 26262−26279.
(53) *baizgroup/cGANN_denoising: Scripts for denoising experimental 2D IR Spectra based on pix2pix*. https://github.com/baizgroup/cGANN_denoising (accessed 2023-08-24).
(54) Donoho, D. L. De-Noising by Soft-Thresholding. *IEEE Trans. Inf. Theory* **1995**, *41* (3), 613−627.

https://doi.org/10.1021/acs.jpca.3c05755
J. Phys. Chem. A 2023, 127, 9853−9862